Adsorption performance and mechanism of U(VI) by hydroxy-aluminum impregnated chitosan

Jinhui Yang[a,*], Chuanshu Li[a,*], Yanghong Dai[b], Bing Yang[c], Jingsong Wang[a], Shukui Zhou[a], Zengjiang Lei[a], Yi Luo[a]

[a]*School of Civil Engineering, Hunan Province Key Laboratory of Pollution Control and Resources Reuse Technology, University of South China, Hengyang 421001, China, Tel. +86 73 48282505; emails: yangjinhui126@126.com (J.H. Yang), 15656534862@163.com (C.S. Li), xhwjs@163.com (J.S. Wang), zhoushukui@usc.edu.cn (S.K. Zhou), 530566791@qq.com (Z.J. Lei), 648949682@qq.com (Y. Luo)*
[b]*CGNPC Nuclear Power Operation Co. Ltd., Shenzhen 518000, China, email: 394859179@qq.com*
[c]*Hunan Nuclear Sanli Technology Engineering Co. Ltd., Hengyang 421001, China, email: 932936624@qq.com*

Received 7 April 2019; Accepted 22 October 2019

ABSTRACT

A novel adsorbent of hydroxy-aluminum impregnated chitosan (Al-CTS) was fabricated via in-situ hydrolysis and impregnation technique for the removal of U(VI) from aqueous solutions in this study. Al-CTS was characterized by scanning electron microscopy (SEM), Fourier transforms infrared spectroscopy and X-ray photoelectron spectroscopy, to explore the adsorption properties and the reaction mechanism of Al-CTS for U(VI). The results showed that hydroxy-aluminum (AlOOH) was successfully loaded on the CTS surface. The consequence revealed that surface complex between Al–O bond, –NH$_2$ group, –OH group and U(VI) may participate in the adsorption processes, and the main mechanism is the surface complexation of the internal sphere. This process fitted well with quasi-second-order kinetic model ($R^2 > 0.99$), Langmuir and Freundlich isothermal model ($R^2 > 0.98$). Compared with CTS, the adsorption capacity of Al-CTS for U(VI) increased by 23.85 mg/g, and the cationic interference degree was small. It is expected to be used to separate and recover uranium from radioactive wastewater.

Keywords: Al-CTS; U(VI); Adsorption performance; Reaction mechanism

1. Introduction

In recent years, with the rapid development of the nuclear industry, the demand for uranium as an important raw material for the nuclear industry is increasing. Meanwhile, the environmental pollution caused by uranium has been paid more and more attention. Low concentration uranium-contained wastewater will inevitably enter the environment along with environmental migration and food chain enrichment, which poses a potential threat to the natural ecological environment and human health [1,2] (affecting the water quality of mining areas, corrosion of pumps, pipelines, and other equipment; teratogenic mutagenesis; affecting the normal growth and activity of animals and plants). How to effectively treat uranium-contained wastewater and recover uranium has become an urgent nuclear environmental problem. At present, the treatment methods of uranium-contained wastewater include chemical precipitation [3], solvent extraction [4], biological treatments [5], membrane separation [6], adsorption [7–9] and zero-valent metal remediation [10].

* Corresponding author.

Among them, the adsorption method has the advantages of high adsorption efficiency, low operation cost, without secondary pollution and reusable adsorbent.

As a highly efficient adsorbent, nano-metal oxides have large specific surface area and high reactivity [11]. The use of nano-metal oxides to adsorb heavy metals in water has gradually become a research hotspot. Among these metal oxides, nanoscale AlOOH shows a good adsorption effect in water treatment. There are a large number of hydroxyl groups on the surface of AlOOH, which has excellent adsorption properties for heavy metals [12,13]. However, due to the fine powder of nanoscale AlOOH, it is difficult to separate and recycle in water, and it is easy to cause secondary pollution, which limits its application in the water treatment process. Therefore, to prepare granular adsorbent materials, researchers mostly use the method of particle carrier modification. The chitosan biopolymer produced by deacetylation of chitin has good hydrophilicity and a stable complex structure with uranyl ions. It is a good adsorbent for uranium separation. Hydroxy-aluminum impregnated chitosan (Al-CTS) adsorbent is prepared by self-crosslinking of chitosan and embedding hydroxy-aluminum into chitosan polymer gel [14]. It can improve the adsorption capacity, selectivity and mechanical strength of chitosan for uranium. It can also solve the problem that AlOOH is a fine powder, which is difficult to separate and recycle in water. It is expected to be used to separate and recover uranium from radioactive wastewater.

Hence, in this study, a novel sorbent of Al-CTS was fabricated via in-situ hydrolysis and impregnation technique for the removal of U(VI) from aqueous solutions. The underlying surface reaction mechanism was carefully characterized by scanning electron microscopy (SEM), Fourier transform infrared spectroscopy (FT-IR) and X-ray photoelectron spectroscopy (XPS) of the samples before and after adsorption. Furthermore, the adsorption behavior of Al-CTS for U(VI) was investigated with respect to different experimental conditions such as initial solution pH, reaction time, ionic strength, temperature, concentration of U(VI), and interfering ions. The regeneration of adsorbents was also considered. The adsorption kinetics and isotherms were conducted to evaluate the adsorption capacity of Al-CTS.

2. Materials and methods

2.1. Chemicals and instruments

2.1.1. Chemicals

Benchmark U_3O_8 (analytical purity) was obtained from the Sixth Institute of Nuclear Industry (Hengyang, China). Chitosan (degree of deacetylation > 95%); aluminum chloride hexahydrate ($AlCl_3 \cdot 6H_2O$), acetic acid (CH_3COOH), hydrochloric acid (HCl), sodium hydroxide (NaOH), silver nitrate ($AgNO_3$), sodium nitrate ($NaNO_3$) are all analytical pure reagents; experimental water is ultrapure water.

2.1.2. Instruments

Electronic constant speed mixer (JHS-1/90 Hangzhou Instrument and Electric Machinery Factory, Hangzhou, China); pH meter (PHS-3C, Shanghai Instrument and Electrical Science Instrument Co. Ltd.); ultraviolet-visible spectrophotometer (UV-2350, Beijing Purkinje General Instrument Co. Ltd., Trading Company, Shanghai, China); scanning electron microscope (JSM-7500F, JEOL Company of Japan); Fourier transform infrared spectrometer (NICOLET 6700, Thermo Fisher Company, USA); XPS photoelectron spectrometer (ESCALAB250, Thermo Fisher Science, USA); zeta potentiometer (ZEN3690, Malvern, UK).

2.2. Material preparation

2.2.1. CTS pretreatment

Chitosan powder was dissolved in 250 mL, 5% acetic acid solution, stirred uniformly at room temperature, aged for 30 min, dried at 338 K for 24 h, and sealed preservation.

2.2.2. Preparation of AlOOH

12.07 g $AlCl_3 \cdot 6H_2O$ was dissolved in 50 mL deionized water. Under the action of continuous heating and stirring, the NaOH solution of 1 M was slowly dripped by the basic burette to form granular spheres. The titration was stopped when the pH value reached 7.0 ± 0.1. Maintained the pH value equilibrium for 30 min, aged for 24 h. The resulting precipitate was filtered while being washed with ultrapure water and repeated several times until no white precipitate formed after the addition of the $AgNO_3$ solution to the filtrate. The filtered cake was put into the oven and dried at 338 K for 24 h [14]. The AlOOH material was obtained.

2.2.3. Preparation of Al-CTS

Under the action of continuous heating and stirring, the pretreated CTS (5 g) was mixed with $AlCl_3 \cdot 6H_2O$ (0.25 M) solution. Then slowly dripped into NaOH (1 M) solution by a basic burette to form granular spheres. The titration was stopped when the pH value reached 7.0 ± 0.1. The remaining steps were the same as 2.2.2.

2.3. Characterizations

The Al-CTS samples before and after adsorption were systematically analyzed by SEM, FT-IR, and XPS. The zeta-potentials of Al-CTS were measured on a nanoscale and zeta potential instrument (ZEN3690, Malvern).

Specifically, zeta-potentials were measured at different pH conditions. The solution pH was adjusted by NaOH (0.1 M) and HCl (0.1 M) and dispersed by ultrasound for 10 min. The Al-CTS (0.5 g) was put into the deionized water and the electrical properties and isoelectric points were analyzed.

2.4. Adsorption performance experiments

To study the adsorption performance of Al-CTS for U(VI), the experiments were carried out in Erlenmeyer Flasks placed in a temperature-controlled orbital shaker at a rate of 160 r/min. First, took 20 mg/L U(VI) standard solution 25 mL in Erlenmeyer Flasks, adjusted initial pH value of the solution with acid (0.1–0.5 M HCl) and base (0.1–0.5 M NaOH). Then added adsorbent (20 mg), oscillated reaction under

constant temperature shaking bed for a while. Finally, the solution became clear after filtration. And determined residual solution U(VI) content by 2-(5-bromo-2-pyridylazo)-5-diethylaminophenol spectrophotometry [15]. According to Eqs. (1) and (2), calculated the adsorption capacity and removal rate of Al-CTS for U(VI). All experiments were performed in duplicate and averaged values were reported.

$$R\left(\%\right) = \frac{\left(C_0 - C_e\right)}{C_0} \times 100 \tag{1}$$

$$Q\left(\text{mg/g}\right) = \frac{\left[\left(C_0 - C_e\right) V\right]}{m} \tag{2}$$

Here R is the removal rate of U(VI), (%); Q is the adsorption capacity of Al-CTS for U(VI), (mg/g); C_0 is the initial concentrations of U(VI), (mg/L); C_e is the equilibrium concentrations of U(VI), (mg/L); V is the volume of solution, (L); m is the mass of adsorbent, (g).

3. Results and analysis

3.1. Adsorption mechanism of U(VI) by Al-CTS

3.1.1. Scanning electron microscopy

The SEM characterization results of CTS (a) and Al-CTS (b) are shown in the figure. As shown in Fig. 1a, CTS is an amorphous spatial network polymer. The surface is smooth and folded, with a large number of slit or wedge-shaped holes. The structure can effectively increase the surface area of the material. From Fig. 1b the smooth surface of Al-CTS shows a nano-sized white granular structure with a diameter of 30–100 nm, irregular shape, an uneven inner surface, and large internal voids. This may be related to the coordination sites between metal and chitosan. Specifically, it can be seen that the AlOOH particles are uniformly loaded on the CTS surface.

3.1.2. Fourier transform infrared spectroscopy

The FT-IR spectra of CTS (a), pre-adsorption Al-CTS (b) and post-adsorption Al-CTS (c) are shown in Fig. 2,

respectively. In the FT-IR spectra of CTS (a), the characteristic broadband near 3,435 cm⁻¹ corresponds to the interaction of the stretching vibration of O–H and N–H in chitosan particles [16]. The absorption peak at 2,875 cm⁻¹ is attributed to the stretching vibration of saturated C–H in chitosan. The characteristic peaks of the chitosan –NH₂ group appear at 3,435 and 1,604 cm⁻¹ [17]. The absorption band at 1,300–1,000 cm⁻¹ is due to the C–O stretching vibration, and the absorption band at 1,081 cm⁻¹ is due to the bending vibration of hydroxyl groups, indicating that there are alcoholic hydroxyl groups in the structure. For the pre-adsorption Al-CTS (b), the absorption peak of O–H shifts at 3,435 cm⁻¹, which may be related to the loading of AlOOH on the CTS surface and the formation of more hydroxyl groups. The peaks at 1,084 cm⁻¹ corresponds to the bending vibration of Al–OH, and the peaks at near 608 and 477 cm⁻¹ are corresponding to Al–O stretching and bending vibrations, concluding that AlOOH has been successfully compounded onto the CTS surface [18].

Analysis and compare pre-adsorption Al-CTS (b) and post-adsorption Al-CTS (c), the results show that Al-CTS migrates greatly at 3,449 and 1,640 cm⁻¹, and the intensity of
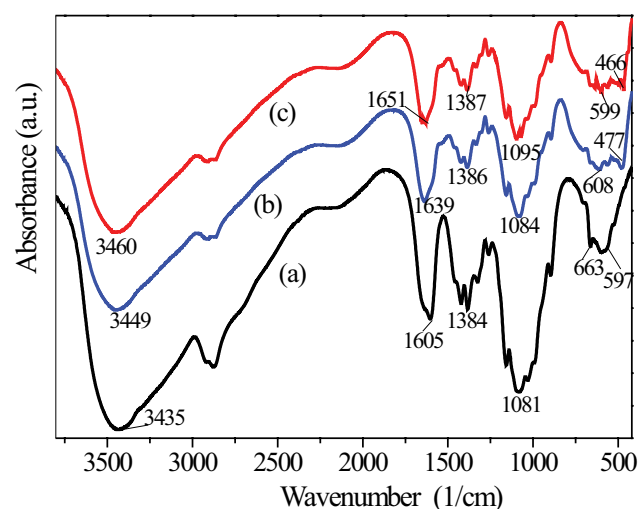
Fig. 2. FT-IR spectra of CTS (a), pre-adsorption Al-CTS (b) and post-adsorption Al-CTS (c).
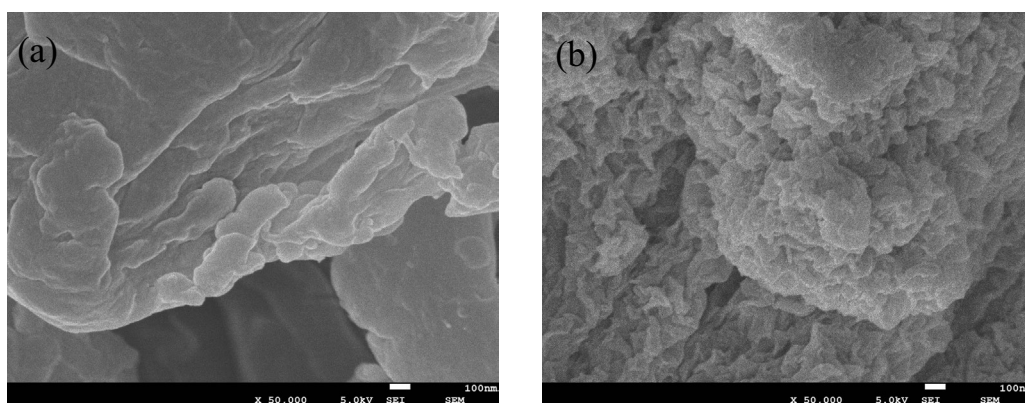
Fig. 1. SEM characterization of CTS (a) and Al-CTS (b).

the peak decreases. This is due to the coordination reaction between N atom in –NH$_2$ group and U(VI) and the formation of the N→U(VI) coordination bond [19]. The bending vibration of O–H corresponding to the absorption peak at 1,084 cm^{-1} has shifted, indicating that hydroxyl groups also participated in the adsorption reaction, thus weakening the vibration intensity of O–H. The corresponding Al–O stretching vibration at 608 and 477 cm^{-1} shift to 599 and 466 cm^{-1}, indicating that surface complexation or ion exchange of U(VI) with Al–O bond may occur during the adsorption process [17,20].

3.1.3. X-ray photoelectron spectroscopy

In this study, the adsorption mechanism of U(VI) by Al-CTS is studied by XPS characterization of Al-CTS before and after adsorption. The characteristic peaks of Al 2p, O 1s, U 4f$_{7/2}$, and N 1s are carefully analyzed by XPS technique. The XPS spectra are as follows:

Fig. 3a shows the XPS spectra of Al 2p before and after adsorption. Al 2p has only one diffraction peak with a binding energy of 73.9 eV, representing hydroxides or oxides of aluminum [21]. This indicates that AlOOH has been successfully loaded on the surface of CTS. After adsorbing U(VI), the peak area of Al–O (73.9 eV) decreases by 19.21%. In addition, O1s before adsorption (Fig. 3b), the peak at 531.6 eV represents the binding energy of Al–O, and the peak at 532.6 eV represents that CTS itself contains C–O–C or C–O–H structure [22]. O 1s after adsorption (Fig. 3c), the peak area of Al–O (531.6 eV) decreases by 18.98%, while the peak area of C–O (532.6 eV) does not change before and after adsorption. The results show that the surface complex
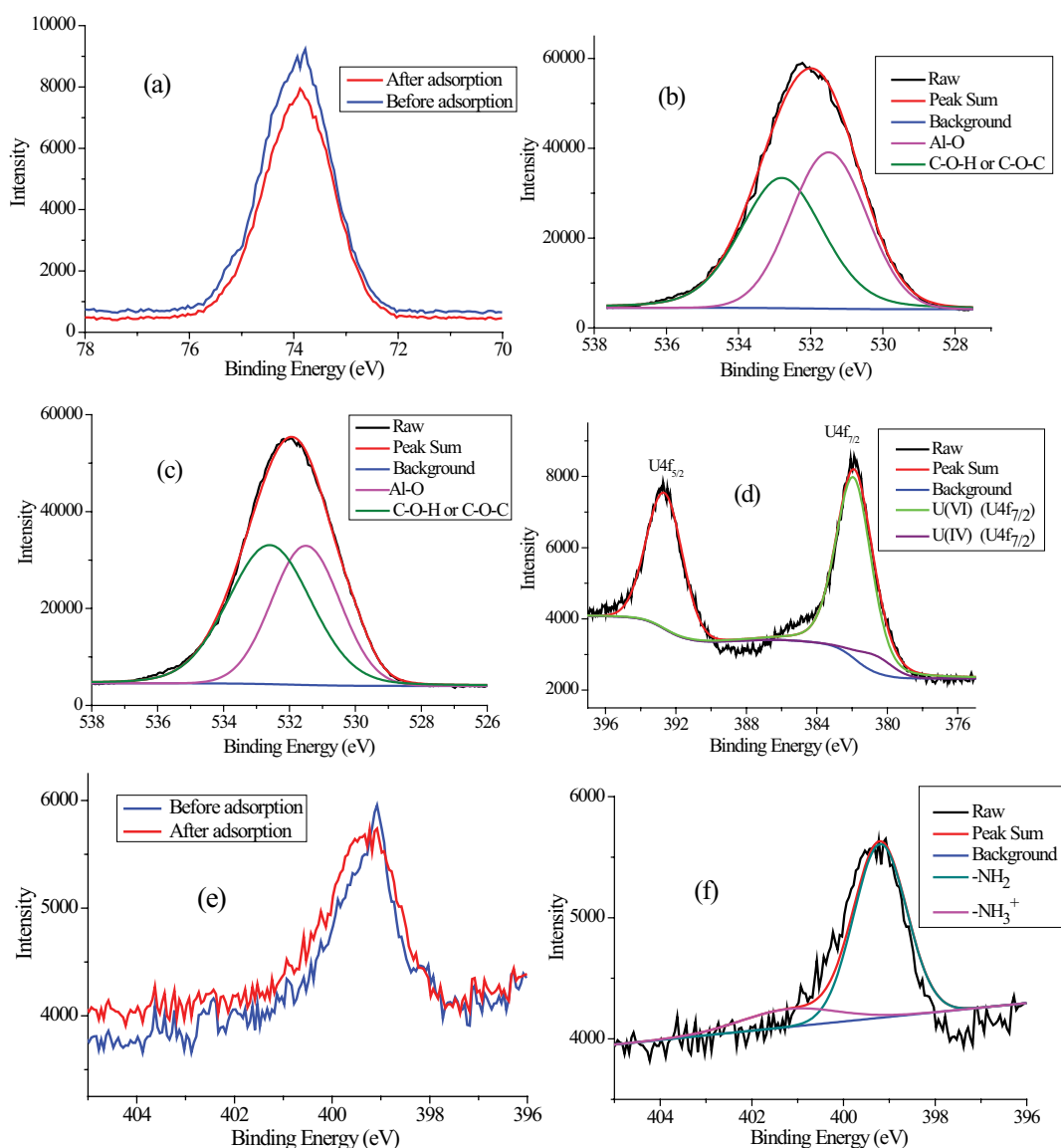
Fig. 3. XPS spectra of the Al-CTS: (a) Al 2p before and after adsorption, (b) O 1s before adsorption, (c) O 1s after adsorption, (d) U 4f after adsorption, (e) N 1s before and after adsorption, and (f) N 1s after adsorption.

between Al–O bond and U(VI) may participate in the adsorption process.

From the XPS results of U 4f in Fig. 3d, it can be seen that the double peaks are due to orbital spin splitting of 4f level electrons in uranium atom, and correspond to U $4f_{7/2}$ and U $4f_{5/2}$, respectively. The peak at $4f_{7/2}$ can be attributed to UO_2 (U(IV)) with a binding energy of 380.3 ± 0.4 eV and UO_3 (U(VI)) with binding energy of 381.6 ± 0.3 eV [23]. From Fig. 3d, the binding energy at U $4f_{7/2}$ is 381.6 eV and at U $4f_{5/2}$ is 392.6 eV, it can be concluded that the uranium is on the Al-CTS surface with U(VI) form. The valence state of uranium has not changed during the removal of U(VI) by Al-CTS. The reaction mechanism is mainly adsorption, and there is a little reduction reaction.

Fig. 3e is the XPS spectra of N 1s before and after adsorption, and Fig. 3f is the peak fitting spectra of N 1s after adsorption. By comparing the XPS spectra of N1s before and after adsorption, it can be found that the N1s peak of Al-CTS is a single peak, and the binding energy is 399.1 eV ($-NH_2$ group). After U(VI) adsorption, a new $-NH_3^+$ group with binding energy of 401.2 eV appears. Compared with 399.1 eV N1s, the new N1s binding energy of 401.2 eV increased by 2.1 eV, which indicates that N tends lone pair electrons being shared, and it is easy to provide lone pair electrons to form complex [24]. The reason for the increase of binding energy may be that $-NH_2$ in CTS provides lone pairs of electrons to form a complex with U(VI) and thus adsorbs U(VI) [25]. This is consistent with FT-IR analysis, indicating that the adsorption of uranium by Al-CTS is due to the coordination of lone pair electron pairs provided by $-NH_2$ with U(VI).

3.1.4. Zeta-potentials

The surface electric property is a dominant factor to affect the sorption behavior of the adsorbent. From Fig. 4, the pHzpc (zero point charge) value is calculated to be 6.2, indicating that the surface property of Al-CTS is positive at pH < 6.2 and carried the negative charge at pH > 6.2.
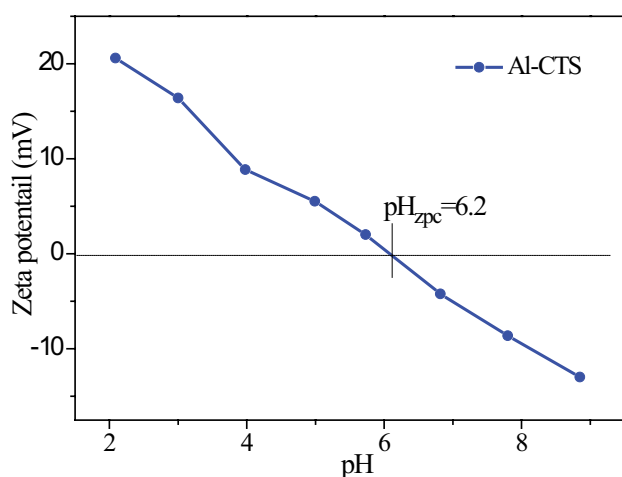
3.2. Adsorption performance of U(VI) by Al-CTS

3.2.1. Effect of initial pH

The effects of CTS, AlOOH, and Al-CTS on the adsorption of U(VI) were investigated under the conditions of solution initial pH in the range of 3.0–8.0, as shown in Fig. 5. Among the three materials, the adsorption effect of AlOOH is relatively poor, the removal rate is only 75.2% at pH 6.0. This indicates that AlOOH has little effect on uranium migration and is not suitable for use as an adsorbent to treat uranium in wastewater. CTS at pH 4.0–5.0 and Al-CTS at pH 6.0–7.0 have a better adsorption effect, the optimum removal rate are 94.7% and 98.6%, respectively. Compared with CTS, because of the amphoteric chemical properties of aluminum, the optimum pH of adsorbing U(VI) by Al-CTS is extended to neutrality, which makes it more practical in the treatment of U(VI) wastewater.

At low pH, uranium ion is mainly in the form of UO_2^{2+}. Competitive adsorption of H^+ and protonation of active sites (hydroxyl and amino groups) may lead to a decrease of U(VI) removal efficiency [26]. As shown in Fig. 4, the zeta potential of Al-CTS indicates that with the increase of pH, the amino group and hydroxyl group are deprotonated gradually. When the pH > pHzpc, the surface charge of Al-CTS becomes negative, and the removal rate tends to decrease. This may be due to the formation of non-complex anion species (such as $(UO_2)OH_3^-$ and $(UO_2)_3OH_7^-$) and these anionic substances repel the negative charge on the adsorbent surface [27]. It is speculated that the adsorption mechanism of uranyl ions is the coordination between uranyl ions and free active sites (deprotonated amines and hydroxyl groups) [17].

Fig. 6 also shows the effect of ionic strength (in the presence of different $NaNO_3$ concentrations) on the adsorption of U(VI) by Al-CTS. The adsorption of U(VI) is hardly affected by the ionic strength at different pH values, suggesting that the main adsorption mechanism is internal sphere surface complexation rather than external sphere surface complexation or ion exchange [17].

Fig. 4. Zeta potentials of Al-CTS varies with pH.
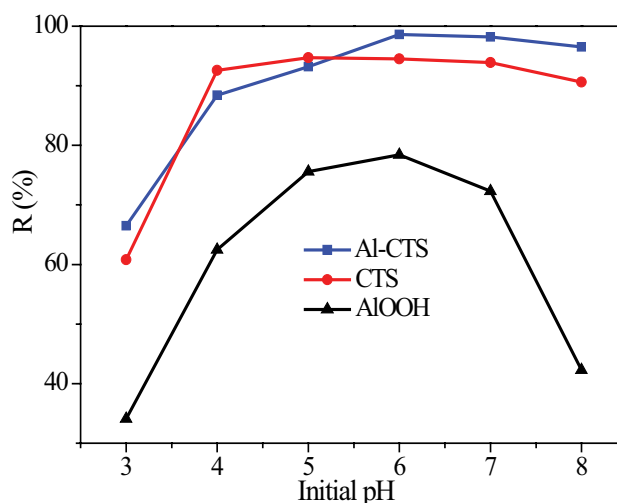
Fig. 5. Effect of initial pH on removal of U(VI) (time = 80 min, T = 298 K, adsorbent dosage = 0.8 g/L, and U(VI) = 20 mg/L).
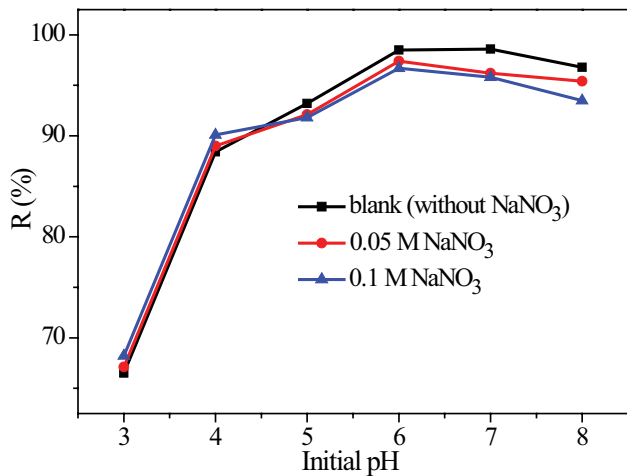
Fig. 6. Effect of ionic strength on removal of U(VI) (time = 80 min, T = 298 K, adsorbent dosage = 0.8 g/L, and U(VI) = 20 mg/L).

Fig. 7. Effect of initial U(VI) concentration on removal of U(VI) (pH = 6.0, time = 80 min, T = 298 K, and adsorbent dosage = 0.8 g/L).

3.2.2. Effect of initial U(VI) concentration

The effects of CTS, AlOOH, and Al-CTS on the adsorption of U(VI) were investigated under the conditions of initial concentration of uranium in the range of 10–120 mg/L, as shown in Fig. 7. The capacity of uranium adsorbed by these three materials increases with the increase of initial uranium concentration. When the initial uranium concentration is more than 50 mg/L, the adsorption capacity of CTS and AlOOH tends to be stable, while the adsorption capacity of Al-CTS continues to increase, up to 82.34 mg/g, which is 23.85 mg/g higher than that of CTS. This is due to the incorporation of the active group (hydroxyl) of fine dispersed AlOOH nanoparticles into the CTS matrix, the adsorption capacity of Al-CTS adsorbent is higher than that CTS microspheres.

3.2.3. Effect of reaction time and reaction kinetics

The effect of reaction time on the U(VI) removal by Al-CTS was investigated with variation of reaction time from 20 to 120 min. As shown in Fig. 8, at the initial stage of the reaction, the removal rate of U(VI) in the solution increases rapidly with the reaction time. With the extension of the reaction time, the removal rate and adsorption capacity increase gradually, but the growth rate slows down. After 60 min, the reaction reached equilibrium, and the maximum adsorption capacity reached 24.65 mg/g.

To intensive study, the reaction kinetic characteristics of Al-CTS on U(VI), the kinetics of U(VI) adsorption by Al-CTS were linearly fitted by pseudo-first-order,

pseudo-second-order and intra-particle diffusion models (Table 1). The three model expressions are as follows:

$$\ln\left(q_e - q_t\right) = \ln q_e - k_1 t \tag{3}$$

$$\frac{t}{q_t} = \frac{1}{k_2 q_e^2} + \frac{t}{q_e} \tag{4}$$

$$q_t = k_{dif} \times t^{1/2} + C \tag{5}$$

Here q_e is the adsorption capacity at equilibrium, (mg/g); q_t is the adsorption capacity at time t, (mg/g); k_1 (1/min), k_2 (g/mg min) and k_{dif} (mg/g min$^{-1/2}$) are respectively the kinetic constants of pseudo-first-order, pseudo-second-order, and intra-particle diffusion models; C is the influence constant of boundary layer thickness on the adsorption process.

Pseudo-second-order kinetic model is used to describe the chemical adsorption behavior of valence bond due to sharing or exchanging electrons in the process of adsorbing nuclide ions between solid and liquid [9,28]. Table 1 shows that the pseudo-second-order kinetic model has the highest correlation coefficient, and the standard deviation between q_e and $q_{e,act}$ (the actual equilibrium adsorption capacity) is only 0.92%. It shows that the pseudo-second-order kinetic model is more suitable for describing the chemical process of uranium adsorption by Al-CTS. In addition, the fitting curve of the intra-particle diffusion model and the intercept of the Y-axis are not zero, which indicates that the adsorption rate

Table 1
Basic parameters of the kinetic model

Kinetic model	q_e	k_1	k_2	k_{dif}	C	R^2
Pseudo-first-order	1.244	0.0211				0.8006
Pseudo-second-order	24.88		0.0402			0.9999
Intra-particle diffusion				0.1482	23.186	0.8316
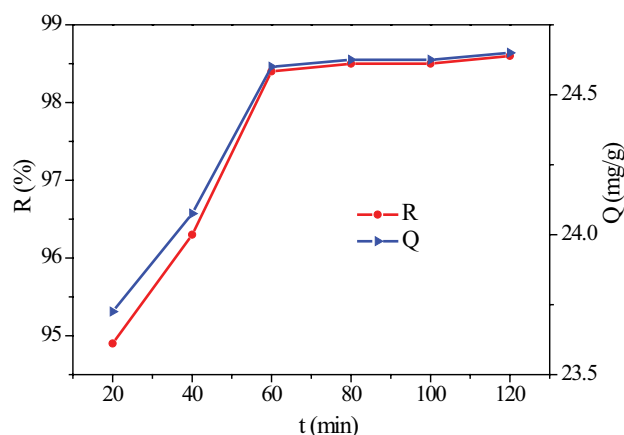
Fig. 8. Effect of reaction time on removal of U(VI) (pH = 6.0, $T = 298$ K, adsorbent dosage = 0.8 g/L, and U(VI) = 20 mg/L).

is not controlled by a single step of intraparticle diffusion, but by multiple adsorption mechanisms [29].

3.2.4. Effect of temperature and adsorption isotherms

At temperatures of 288, 298, and 308 K, investigated the effects of Al-CTS on the removal of U(VI) respectively. As shown in Fig. 9, when the initial concentration of U(VI) is low, the three curves coincide basically, indicating that the temperature change has a little effect on the adsorption of U(VI). When the concentration of U(VI) continues to increase, the distance between the temperature curve of 288 K and the curve of 298 K gradually increases. And with the increase of temperature, the adsorption capacity corresponding to each concentration increases slightly, which indicates that the adsorption process is endothermic, and the increase of temperature can promote the adsorption of U(VI) [30]. The distance between the temperature curve of 298 K and the curve of 308 K is very small, it is indicated that continuous increase of temperature has no obvious effect on the adsorption of U(VI).

The experimental data were fitted according to Langmuir and Freundlich isotherm equations. The equations are as follows, and the fitting parameters are shown in Table 2. The Langmuir model assumes that the removal of adsorbate occurs on an energetically homogenous surface through monolayer adsorption, and the Freundlich model is derived by assuming multilayer adsorption with a non-uniform distribution of adsorption heat and affinity over the heterogeneous surface [31,32].
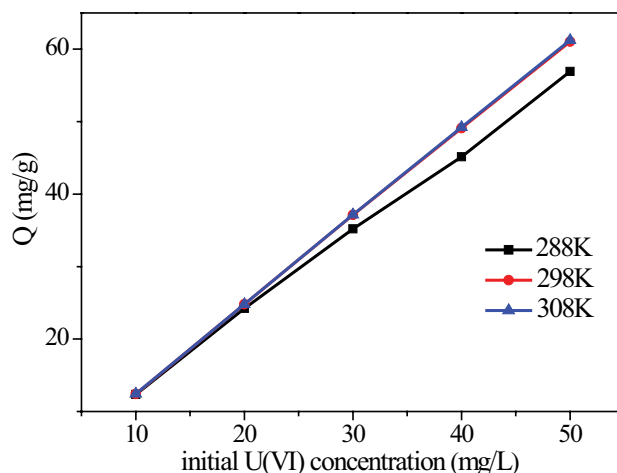
Fig. 9. Adsorption isotherms at different temperatures (pH = 6.0, time = 80 min, adsorbent dosage = 0.8 g/L, and U(VI) = 10–50 mg/L).

$$\frac{C_e}{q_e} = \frac{C_e}{q_{max}} + \frac{1}{bq_{max}} \tag{6}$$

$$\ln q_e = \ln K_F + \ln \frac{C_e}{n} \tag{7}$$

Here C_e is the equilibrium concentration of U(VI) in solution, (mg/L); q_e is the equilibrium adsorption capacity of U(VI), (mg/g); q_{max} is the maximum saturated adsorption capacity, (mg/g); b is the adsorption equilibrium constant, (L/mg); K_F is the adsorption coefficient, (mg^{1-n} L^n/g); n is the adsorption strength constant.

According to the data in Table 2, Langmuir and Freundlich adsorption isotherm models can well fit the adsorption results. The correlation coefficients ($R_1^2 > R_2^2$) indicates that the Langmuir model is the main adsorption model of the composites. It suggests that mono-layer chemical adsorption is dominated in the adsorption of U(VI) onto Al-CTS. The maximum adsorption capacity (q_{max}) is found to be 77.52 mg/g for U(VI) at 308 K. The maximum adsorption capacities of various chitosan-based adsorbents for U(VI) are shown in Table 3. Among them, the adsorption capacity of Al-CTS adsorbent has certain competitive advantages. In addition, in the Freundlich model, the n values at all three temperatures are greater than 1, which indicates that the adsorption process is preferential and the adsorption capacity of Al-CTS is large [37].

Table 2
Isotherm model fitting parameters

T (K)	Langmuir			Freundlich		
	q_{max} (mg/g)	b (L/mg)	R_1^2	K_F (mg^{1-n} L^n/g)	n	R_2^2
288	67.11	1.242	0.9893	28.628	2.525	0.9877
298	76.34	3.046	0.9908	60.443	1.909	0.9770
308	77.52	3.308	0.9903	65.385	1.8815	0.9809

Table 3
Comparison of adsorption capacities of various chitosan-based adsorbents for U(VI)

Adsorbents	Adsorption capacities (mg/g)	References
Chitosan impregnated with magnetite nanoparticles	42.0	[33]
Chitosan hydrogel	68.0	[34]
Chitosan/poly(acrylamide) hydrogel	73.0	[35]
Ethylenediamine-modified magnetic chitosan	82.83	[36]
Pre-treated chitosan	53.67	This work
Hydroxy-aluminum impregnated chitosan	77.52	This work

3.2.5. Effect of interfering ions

In the actual wastewater treatment, there are many other anions and cations in the wastewater. When the initial concentration of U(VI) was 50 mg/L, the pH was 6.0, the adsorbent dosage was 20 mg, the temperature is 298 K, and the reaction time is 80 min, the effects of common cations Ca^{2+}, Zn^{2+}, Fe^{2+}, Mn^{2+}, Cu^{2+}, Cr^{6+} on the adsorption of U(VI) by Al-CTS were discussed.

From Fig. 10, the results show that with the increase of the concentration of interfering ions, Fe^{3+} promoted the adsorption of U(VI) on Al-CTS. This is due to the complexation reaction between U(VI) and the hydrolysate of Fe^{3+} under weakly acidic conditions (the reaction equation (8)). The effect of Zn^{2+} on the adsorption of U(VI) is not obvious, but Mn^{2+}, Cu^{2+}, Cr^{6+} have an inhibitory effect on the adsorption, of which Cu^{2+} has the greatest inhibitory effect, follows by Ca^{2+}, Mn^{2+}, Cr^{6+}. It shows that Cu^{2+} and uranyl ions have the same adsorption sites and have strong competitive adsorption [23]. Overall, within a certain concentration range, the presence of six cations has little effect on the adsorption performance of Al-CTS, which ensures the good application potential and prospect of Al-CTS in wastewater treatment.

$$FeOH + UO_2(OH)^+ \rightarrow FeOUO_2OH + H^+ \qquad (8)$$

3.2.6. Reusability experiments

Reusability experiments were conducted to test the stability and reusability of Al-CTS. According to the above experiments, the removal rate of U(VI) by Al-CTS was low under strong acid conditions, so used 0.1 M HCl solution as desorbent. the Al-CTS after adsorption was put into 0.1 M HCl solution for 6 h, then the sample was washed with ultrapure water and absolute alcohol three times, respectively. After vacuum drying, the adsorption experiments were carried out, and the above steps were repeated several times under the same conditions. As shown in Fig. 11, after three repeated uses, the removal rate of U(VI) by Al-CTS decreased slightly, but still exceeded 90%. This indicates that Al-CTS is a reusable adsorbent.

3.3. Adsorption mechanism of U(VI) by Al-CTS

According to the above analysis, the mechanism of adsorption of U(VI) by Al-CTS includes two steps: firstly, uniformly dispersed AlOOH nanoparticles are formed in the chitosan matrix, secondly, U(VI) adsorbed into Al-CTS
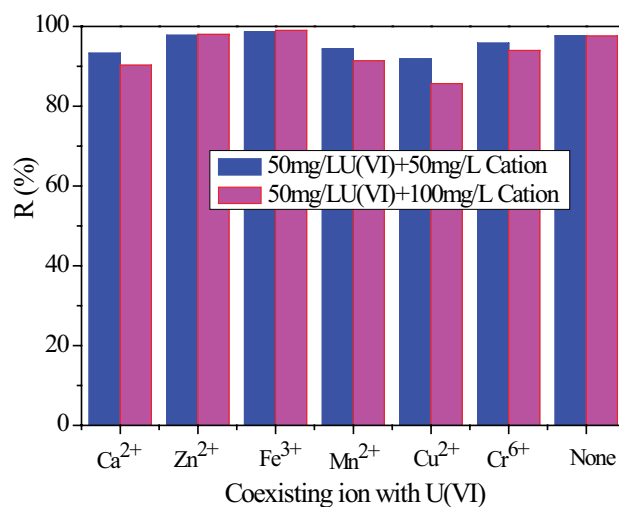
Fig. 10. Effect of interfering ions on removal of U(VI) (pH = 6.0, T = 298 K, time = 80 min, adsorbent dosage = 0.8 g/L, and U(VI) = 20 mg/L).
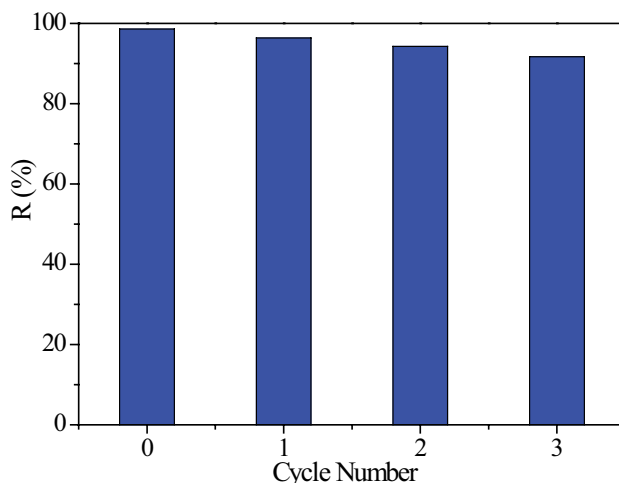
Fig. 11. Recycling of Al-CTS on the removal of U(VI).

sorbents. The FT-IR and XPS consequence reveal that surface complex between Al–O bond, –NH$_2$ group, –OH group and U(VI) may participate in the adsorption processes. The ionic strength result suggests that the main adsorption mechanism

is an internal sphere surface complexation rather than external sphere surface complexation or ion exchange. U(VI) is strongly adsorbed on Al-CTS as an inner-complex through surface complexation with the Al–O bond. At the same time, Al-CTS provides enough active sites (–NH$_2$ group, –OH group) to chelate U(VI).

4. Conclusions

In this study, Al-CTS was successfully fabricated via the in-situ hydrolysis and impregnation technique. Compared with CTS, the adsorption capacity of U(VI) by Al-CTS was greatly improved, and the adsorption capacity was increased by 23.85 mg/g. By investigating the adsorption performance of Al-CTS for U(VI), the optimum adsorption conditions were determined: the initial concentration of U(VI) was 10–50 mg/L, the initial pH of solution was 6.0, the dosage was 20 mg, the temperature was 298 K, and the reaction time was 80 min, the removal rate of Al-CTS on U(VI) was above 95%. In addition, the adsorption of U(VI) by Al-CTS had good regeneration and the cationic interference degree was small. The adsorption process followed a quasi-second-order kinetic model, indicating that the adsorption was mainly controlled by chemical action. The high value of the correlation coefficient for the Langmuir isotherms suggests that adsorption occurs through homogeneous and monolayer adsorption. FT-IR and XPS analysis show that surface complex between Al–O bond, –OH group, –NH$_2$ group and U(VI) may participate in the adsorption processes, and the main mechanism is the surface complexation of the internal sphere.

Acknowledgments

References

[1] J.H. Zhu, Q. Liu, J.Y. Liu, R.R. Chen, H.S. Zhang, J. Yu, M.L. Zhang, R.M. Li, J. Wang, A novel ion-imprinted carbon material induced by hyperaccumulation pathway for the selective capture of uranium, ACS Appl. Mater. Interfaces, 34 (2018) 28877–28886.

[2] Y. Xie, C.L. Chen, X.M. Ren, X.X. Wang, H.Y. Wang, X.K. Wang, Emerging natural and tailored materials for uranium-contaminated water treatment and environmental remediation, Prog. Mater. Sci., 103 (2019) 180–234.

[3] D.K. Singh, K.N. Hareendran, T. Sreenivas, V. Kain, G.K. Dey, Development of a phosphate precipitation method for the recovery of uranium from lean tenor alkaline leach liquor, Hydrometallurgy, 171 (2017) 228–235.

[4] A.H. Orabi, E.M. El-Sheikh, A.R. Mowafy, M. Abdel-Khalek, M.Y. El Kady, Studies on the selectivity of cetrimide for uranium extraction from wet process phosphoric acid, Int. J. Miner. Process., 137 (2015) 26–33.

[5] M. Stylo, D.S. Alessi, P.Y. Shao, J.S. Lezama-Pacheco, J.R. Bargar, R. Bernier-Latmani, Biogeochemical controls on the product of microbial U(VI) reduction, Environ. Sci. Technol., 47 (2013) 12351–12358.

[6] J.J. Shen, A. Schäfer, Removal of fluoride and uranium by nanofiltration and reverse osmosis: a review, Chemosphere, 117 (2014) 679–691.

[7] H.J. Liu, Y.C. Zhou, Y.B. Yang, K. Zou, R.J. Wu, K. Xie, S.B. Xie, Synthesis of polyethylenimine/graphene oxide for the adsorption of U(VI) from aqueous solution, Appl. Surf. Sci., 471 (2019) 88–95.

[8] C. Christou, K. Philippou, T. Krasia-Christoforou, I. Pashalidis, Uranium adsorption by polyvinylpyrrolidone/chitosan blended nanofibers, Carbohydr. Polym., 219 (2019) 298–305.

[9] Z. Akbari-Jonoush, S. Naseri, M. Farzadkia, H. Mohajerani, M. Shirzad-Siboni, J. Yang, Application of C$_{14}$/SiO$_2$–Fe$_3$O$_4$ and AC–Fe$_3$O$_4$ nanocomposite for U(VI) removal, Desal. Wat. Treat., 57 (2016) 22519–22532.

[10] S. Yan, B. Hua, Z. Bao, J. Yang, C. Liu, B. Deng, Uranium (VI) removal by nanoscale zerovalent iron in anoxic batch systems, Environ. Sci. Technol., 44 (2010) 7783–7789.

[11] R. Bhateria, R. Singh, A review on nanotechnological application of magnetic iron oxides for heavy metal removal, J. Water Process Eng., 31 (2019) 100845.

[12] Z.Y. Xia, L. Baird, N. Zimmerman, M. Yeager, Heavy metal ion removal by thiol functionalized aluminum oxide hydroxide nanowhiskers, Appl. Surf. Sci., 416 (2017) 565–573.

[13] B.L. Sun, X. Li, R. Zhao, M.Y. Yin, Z.X. Wang, Z.Q. Jiang, C. Wang, Hierarchical aminated PAN/γ–AlOOH electrospun composite nanofibers and their heavy metal ion adsorption performance, J. Taiwan Inst. Chem. Eng., 62 (2016) 219–227.

[14] W. Tan, Y.H. Zhang, Y. Szeto, L.B. Liao, A novel method to prepare chitosan/montmorillonite nanocomposites in the presence of hydroxy-aluminum oligomeric cations, Compos. Sci. Technol., 68 (2008) 2917–2921.

[15] T.M. Florence, D.A. Johnson, Y.J. Farrar, Spectrophotometric determination of uranium (VI) with 2-(2-pyridylazo)-5-diethylaminophenol, Anal. Chem., 41 (1969) 1652–1654.

[16] L. Sheng, L. Zhou, Z. Huang, Z. Liu, Q. Chen, G. Huang, A.A. Adesina, Facile synthesis of magnetic chitosan nanoparticles functionalized with N/O-containing groups for efficient adsorption of U(VI) from aqueous solution, J. Radioanal. Nucl. Chem., 310 (2016) 1361–1371.

[17] L.M. Zhou, Z. Li, K. Zeng, Q.S. Chen, Y. Wang, Z.R. Liu, A.A. Adesina, Immobilization of in-situ formed Ni(OH)$_2$ nanoparticles in chitosan beads for efficient removal of U(VI) from aqueous solutions, J. Radioanal. Nucl. Chem., 314 (2017) 467–476.

[18] T. Shi, X.Z. Guo, H. Yang, Preparation and characterization of transparent boehmite (γ-AlOOH) sol, Rare Met. Mater. Eng., 37 (2008) 73–75.

[19] C.C. Ding, W.C. Cheng, X.Q. Nie, Z.W. Niu, T. Duan, Y.Y. Zhang, A.M. Asiri, H.M. Marwani, Y. Li, Y.B. Sun, Spectroscopic and theoretical investigation on efficient removal of U(VI) by amine-containing polymers, Chem. Eng. J., 367 (2019) 94–101.

[20] A.A. Elabd, W.I. Zidan, M.M. Abo-Aly, E. Bakier, M.S. Attia, Uranyl ions adsorption by novel metal hydroxides loaded Amberlite IR120, J. Environ. Radioact., 134 (2014) 99–108.

[21] K.Z. Liu, L.Z. Luo, W. Zhou, J.R. Yang, H. Xiao, Z.L. Hong, H. Yang, Study of behaviors of aluminum overlayers deposited on uranium via AES, EELS, and XPS, Appl. Surf. Sci., 270 (2013) 184–189.

[22] K.R. Zhu, C.L. Chen, H.Y. Wang, Y. Xie, M. Wakeel, A. Wahid, X.D. Zhang, Gamma-ferric oxide nanoparticles decoration onto porous layered double oxide belts for efficient removal of uranyl, J. Colloid Interface Sci., 535 (2019) 265–275.

[23] J.X. Liu, S.B. Xie, Y.H. Wang, Y.J. Liu, P.L. Cai, X. Xiong, W.T. Wang, U(VI) reduction by Shewanella oneidensis mediated by anthraquinone-2-sulfonate, Trans. Nonferrous Met. Soc. China, 25 (2015) 4144–4150.

[24] L. Lei, S.Y. Huang, T. Wen, R. Ma, L. Yin, J.X. Li, Z.S. Chen, T. Hayat, B.W. Hu, X.K. Wang, Fabrication of carboxyl and amino functionalized carbonaceous microspheres and their enhanced adsorption behaviors of U(VI), J. Colloid Interface Sci. 543 (2019) 225–236.

[25] Z.W. Huang, Z.J. Li, L.R. Zheng, L.M. Zhou, Z.F. Chai, X.L. Wang, W.Q. Shi, Interaction mechanism of uranium(VI) with three-dimensional graphene oxide-chitosan composite: insights from batch experiments, IR, XPS, and EXAFS spectroscopy, Chem. Eng. J., 328 (2017) 1066–1074.

[26] G.W. Peng, D.X. Ding, F.Z. Xiao, X.L. Wang, N. Hun, Y.D. Wang, Y.M. Dai, Adsorption of uranium ions from aqueous solution by amine group functionalized magnetic Fe_3O_4 nanoparticle, J. Radioanal. Nucl. Chem., 301 (2014) 781–788.

[27] S. Song, S. Zhang, S.Y. Huang, R. Zhang, L. Yin, Y.Z. Hu, T. Wen, L. Zhuang, B.W. Hu, X.K. Wang, A novel multi-shelled $Fe_3O_4@MnO_x$ hollow microspheres for immobilizing U(VI) and Eu(III), Chem. Eng. J., 355 (2019) 697–709.

[28] Y. Tan, M. Chen, Y. Hao, High effificient removal of Pb(II) by amino-functionalized Fe_3O_4 magnetic nano-particles, Chem. Eng. J., 191 (2012) 104–111.

[29] M. Mazarji, B. Aminzadeh, M. Baghdadi, A. Bhatnagar, Removal of nitrate from aqueous solution using modified granular activated carbon, J. Mol. Liq., 233 (2017) 139–148.

[30] F.Q. Ma, B.R. Dong, Y.Y. Gui, M. Cao, L. Han, C.S. Jiao, H.T. Lv, J.J. Hou, Y. Xue, Adsorption of low-concentration uranyl ion by amidoxime polyacrylonitrile fibers, Ind. Eng. Chem. Res., 57 (2018) 17384–17393.

[31] K. Foo, B. Hameed, Insights into the modeling of adsorption isotherm systems, Chem. Eng. J., 156 (2010) 2–10.

[32] D. Nibou, S. Khemaissia, S. Amokrane, M. Barkat, S. Chegrouche, A. Mellah, Removal of UO_2^{2+} onto synthetic NaA zeolite. Characterization, equilibrium and kinetic studies, Chem. Eng. J., 172 (2011) 296–305.

[33] L.C. Stopa, M. Yamaura, Uranium removal by chitosan impregnated with magnetite nanoparticles: adsorption and desorption, Int. J. Nucl. Energy Sci. Technol., 5 (2010) 283–289

[34] K. Mishima, X. Du, N. Miyamoto, Experimental and theoretical studies on the adsorption mechanisms of uranium(VI) ions on chitosan, J. Funct. Biomater., 9 (2018) 49–59.

[35] R. Akkaya, U. Ulusoy, Adsorptive features of chitosan entrapped in polyacrylamide hydrogel for Pb^{2+}, UO_2^{2+}, and Th^{4+}, J. Hazard. Mater., 151 (2008) 380–388.

[36] J. Wang, R. Peng, J. Yang, Y. Liu, X. Hu, Preparation of ethylenediamine-modified magnetic chitosan complex for adsorption of uranyl ions, Carbohydr. Polym., 4 (2011) 1169–1175.

[37] R. Donat, N. Guy, H. Cetisli, Sorption isotherms and characteristics of U(VI) ion onto composite adsorbent, Desal. Wat. Treat., 30 (2011) 186–194.